Numerical Computation of Flows with Moving Boundaries Using an Immersed Interface Method

Caesar O. HARAHAP and Hideaki MIURA[1)]

The Graduate University for Advanced Studies(SOKENDAI), Toki 509-5292, Japan

[1)]National Institute for Fusion Science, Toki 509-5292, Japan

(Received: 5 September 2008 / Accepted: 21 January 2009)

Aiming at simulating the dynamics of plasma consisting of multiple phases, a new immersed interface method (IIM) scheme to solve multiphase flows with viscosity and density jumps is being developed. A numerical technique to solve the equations of the jump conditions is developed. The validity of the formulations and the numerical technique is confirmed by a numerical test.

Keywords: discontinuity, jump conditions, immersed interface method, iterative method

1. Introduction

Complex behaviors of a thermal plasma in a magnetic confinement device such as the Large Helical Device (LHD) have been studied through numerous Magneto-hydrodynamics (MHD) simulations. (See Refs.[1,2], for example). In numerical studies of a thermal plasma, there are increasing requirements to study peripheral regions and hot plasma core simultaneously. One typical approach for this purpose is to describe the vacuum region by MHD equations with very low pressure and/or mass density, assuming very high resistivity and/or viscosity in the low pressure region. However, numerical oscillations often result from the jumps of physical quantities such as mass density, pressure and temperature. Although it is possible to avoid such oscillations by using numerical techniques such as the Godunov/CIP or TVD schemes (for example, see Refs.[3,4]), it often complicates the computation program and obscures the numerical accuracy.

An alternative simulation approach which can avoid some of the difficulties is found in the Immersed Interface Method (IIM). The IIM is a class of numerical methods for solving differential equations that involve complex interfaces. The IIM can capture discontinuities in the solution and the flux accurately, preserving the sharpness of the interface. Originally developed for solving elliptic equations such as Poisson equations, it has been extended and applied to various other problems including the simulation of incompressible flows with moving interfaces [5]. The IIM has the following essential properties [5]: (1) jump conditions are either known from physical reasoning or derived from the governing equations, and (2) using the jump conditions, finite difference approximations at grid points near the interface are modified.

In the IIM, it is assumed that there is a surface separating two regions or two fluids that the fluid(s) cannot flow across (for two-dimensional flows, a curve). We refer to the surface as the singular surface. On this singular surface, a singular force such as surface tension or elastic tension acts. In plasma dynamics, the cage of magnetic field lines separating the hot plasma core from the peripheral regions can be modeled as a singular surface.

Recently, an IIM technique to solve the incompressible flow of a neutral fluid separated into two regions by a singular surface was developed by Xu and Wang [6,7]. Although they have shown that the IIM can work well to simulate fluid motions, their formulations and techniques are limited to flows with uniform viscosity and density. Since our final objective is to apply the IIM to fusion plasma simulations, it is essential to provide formulae valid for flows with viscosity and/or density jumps. The jump conditions in a multiphase incompressible flow, where the viscosity and the mass density jump across the singular surface, were derived in Ref.[8]. In the present paper, we restrict ourselves on the IIM for the neutral fluid system because the equations of motions are much simpler than those in the MHD equations, and develop a numerical technique to solve the equations of the jump conditions derived there. The jump conditions obtained are then used for computing derivatives according to the IIM discretization scheme. Our technique can be used to develop a scheme for solving non-steady multiphase flows.

2. Governing Equations and IIM Discretization

We concentrate on two-dimensional (2D) flows of two different fluids separated by a closed curve. A schematic description of the model is given in Fig.1. The fluid density ρ and the viscosity μ are piecewise constant in Ω^+ and Ω^-. A singular force acts on the closed curve C ,sustaining the separation of the two fluids.

author's e-mail:harahap.caesar@LHD.nifs.ac.jp

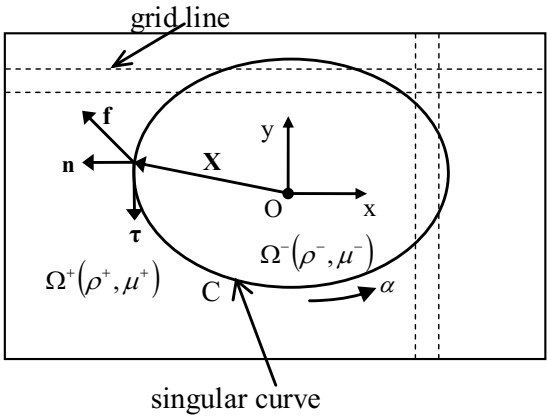

Fig.1 Schematic description of two fluids separated by a singular curve.

The nondimensional incompressible Navier-Stokes equations including a singular force are

$$\rho\left(\frac{\partial \mathbf{u}}{\partial t}+(\mathbf{u}\bullet\nabla)\mathbf{u}\right)=-\nabla p+\frac{1}{\mathrm{Re}}\nabla\bullet\left(\mu\nabla\mathbf{u}+\mu(\nabla\mathbf{u})^T\right)+\mathbf{F}\ , \tag{1}$$

$$\nabla\bullet\mathbf{u}\ =\ 0\ , \tag{2}$$

where $\mathbf{u}$ is velocity, p is pressure, t is time, Re is the Reynolds number, and $\mathbf{F}$ is the singular force. Denoting the coordinates of the curve C by $\mathbf{X}$, the singular force is given by

$$\mathbf{F}=\int_C \mathbf{f}(\alpha,t)\,\delta(\mathbf{x}-\mathbf{X}(\alpha,t))\,d\alpha\ , \tag{3}$$

where α is a Lagrangian parameter parametrizing the curve at a reference time, $\mathbf{f}(\alpha,t)$ is the curve force density, and $\delta(\mathbf{x}-\mathbf{X}(\alpha,t))$ is a two-dimensional Dirac delta function. Since the singular curve moves with the local fluid velocity, the time evolution of $\mathbf{X}(\alpha,t)$ is governed by the following equation

$$\frac{\partial \mathbf{X}(\alpha,t)}{\partial t}\ =\ \mathbf{u}(\mathbf{X}(\alpha,t),t)\,. \tag{4}$$

Taking the divergence of eq. (1), the following Poisson equation for the pressure is obtained.

$$\nabla^2 p=\ \nabla\bullet\mathbf{F}+\frac{1}{\mathrm{Re}}\nabla\bullet\left\{\nabla\bullet\left(\mu\nabla\mathbf{u}\right)+\nabla\bullet\left(\mu\nabla\mathbf{u}\right)^T\right\}-\nabla\bullet\left(\rho\frac{D\mathbf{u}}{Dt}\right)\ , \tag{5}$$

where $\frac{D}{Dt}=\frac{\partial}{\partial t}+\mathbf{u}\bullet\nabla\,.$

The IIM finite difference discretization developed by Xu and Wang [6] can be used to solve these governing equations numerically on a fixed Cartesian mesh. Here, the IIM discretization is described briefly. The derivation can be found in Ref.[6].

Let $\phi(x)$ be a function that is smooth except at discontinuity points ξ and η. Let the variable x be dicretized equidistantly, and the discontinuity points be located at $x_{i-1}<\xi<x_i$ and $x_i<\eta<x_{i+1}$. Then, the first and second derivatives of $\phi(x)$ at x_i are given by

$$\frac{d\phi(x_i)}{dx}=\frac{\phi(x_{i+1})-\phi(x_{i-1})}{2h}-\frac{1}{2h}\left(\sum_{n=0}^{2}\frac{\left[\phi^{(n)}(\xi)\right]}{n!}(x_{i-1}-\xi)^n+\sum_{n=0}^{2}\frac{\left[\phi^{(n)}(\eta)\right]}{n!}(x_{i+1}-\eta)^n\right)+O(h^2)\,, \tag{6}$$

$$\frac{d^2\phi(x_i)}{dx}=\frac{\phi(x_{i+1})-2\phi(x_i)+\phi(x_{i-1})}{h^2}+\frac{1}{h^2}\left(\sum_{n=0}^{3}\frac{\left[\phi^{(n)}(\xi)\right]}{n!}(x_{i-1}-\xi)^n-\sum_{n=0}^{3}\frac{\left[\phi^{(n)}(\eta)\right]}{n!}(x_{i+1}-\eta)^n\right)+O(h^2)\,, \tag{7}$$

where $h=x_i-x_{i-1}=x_{i+1}-x_i$, and $[*]=*^+-*^-$ denotes the jump of a quantity $*$ across a discontinuity (the jump condition for a quantity).

The spatial derivatives appearing in the governing equations can be approximated using eqs. (6) and (7), only if the jump conditions for the velocity, pressure, and their first and second order spatial derivatives are known. Thus, to solve the governing equations by the IIM, it is necessary to obtain these jump conditions.

3. Equations of the Jump Conditions and Numerical Technique to Solve Them

To simplify the eventual technique to solve the equations of the jump conditions, we transform the velocity into a scaled velocity defined as

$$\mathbf{v}\equiv\mu\,\mathbf{u}\,, \tag{8}$$

with components denoted by

$$\mathbf{v}=(u,v)\,. \tag{9}$$

Moreover, we introduce augmented variables defined only on the singular curve C

$$(q_x(\alpha,t),q_y(\alpha,t))=((u^+-u^-),(v^+-v^-))\,, \tag{10}$$

where the superscript + (or -) denotes the Ω^+ (or Ω^-) side. Using the scaled velocity, the Navier-Stokes equation and the pressure Poisson equation are given by

$$\frac{\rho}{\mu}\frac{\partial\mathbf{v}}{\partial t}+\frac{\rho}{\mu^2}(\mathbf{v}\bullet\nabla)\mathbf{v}=-\nabla p+\frac{1}{\mathrm{Re}}\Delta\mathbf{v}\,, \tag{11}$$

$$\nabla^2 p=-\frac{\rho}{\mu}\frac{\partial D}{\partial t}-\frac{\rho}{\mu^2}\nabla\bullet(\mathbf{v}D)+2\frac{\rho}{\mu^2}\left(\frac{\partial u}{\partial x}\frac{\partial v}{\partial y}-\frac{\partial u}{\partial y}\frac{\partial v}{\partial x}\right)+\frac{1}{\mathrm{Re}}\Delta D\,, \tag{12}$$

for $\mathbf{x}\notin C$, where $D=\nabla\bullet\mathbf{v}$.

We also introduce quantities related to the geometry of curve C. Henceforth, let subscript x (or y) denote the x (or y) component of a vector. The tangent vector $\boldsymbol{\tau}_\alpha$, the unit tangent vector $\boldsymbol{\tau}$, and the unit normal vector $\mathbf{n}$ are given by

$$\boldsymbol{\tau}_\alpha=\frac{\partial\mathbf{X}}{\partial\alpha},\qquad J=|\boldsymbol{\tau}_\alpha|,\qquad \boldsymbol{\tau}=\frac{\boldsymbol{\tau}_\alpha}{J}, \tag{13}$$

$$\mathbf{n} = \left(\tau_y, -\tau_x\right). \tag{14}$$

See Fig.1 for a schematic description.

In Ref.[8], the systems of equations of the jump conditions in three-dimensional (3D) flows were derived analytically. The equations in 2D flows can be obtained from the equations in 3D flows by considering one coordinate direction as uniform. Denoting the jump condition of a quantity ψ by

$$[\psi](\alpha,t) = \psi^{+}(\mathbf{X}(\alpha,t),t) - \psi^{-}(\mathbf{X}(\alpha,t),t), \tag{15}$$

they are given as follows:

$$[u] = q_x, \quad [v] = q_y, \tag{16}$$

$$\begin{pmatrix} \tau_{\alpha x} & \tau_{\alpha y} & 0 & 0 \\ 2n_x & n_y & n_y & 0 \\ 0 & 0 & \tau_{\alpha x} & \tau_{\alpha y} \\ 0 & n_x & n_x & 2n_y \end{pmatrix} \begin{pmatrix} \left[\partial u/\partial x\right] \\ \left[\partial u/\partial y\right] \\ \left[\partial v/\partial x\right] \\ \left[\partial v/\partial y\right] \end{pmatrix} = \begin{pmatrix} \partial q_x/\partial\alpha \\ R_{vx} \\ \partial q_y/\partial\alpha \\ R_{vy} \end{pmatrix}, \tag{17}$$

$$[p] = R_p, \tag{18}$$

$$\begin{pmatrix} \tau_{\alpha x} & \tau_{\alpha y} \\ n_x & n_y \end{pmatrix} \begin{pmatrix} \left[\partial p/\partial x\right] \\ \left[\partial p/\partial y\right] \end{pmatrix} = \begin{pmatrix} \partial R_p/\partial\alpha \\ R_{pn} \end{pmatrix}, \tag{19}$$

$$\begin{pmatrix} \tau_{\alpha x}^{\,2} & 2\tau_{\alpha x}\tau_{\alpha y} & \tau_{\alpha y}^{\,2} \\ 2n_x\tau_{\alpha x} & 2n_x\tau_{\alpha y} + n_y\tau_{\alpha x} & n_y\tau_{\alpha y} \\ 1 & 0 & 1 \\ 0 & 0 & 0 \\ 0 & n_x\tau_{\alpha x} & n_x\tau_{\alpha y} \\ 0 & 0 & 0 \end{pmatrix}$$

$$\begin{pmatrix} 0 & 0 & 0 \\ n_y\tau_{\alpha x} & n_y\tau_{\alpha y} & 0 \\ 0 & 0 & 0 \\ \tau_{\alpha x}^{\,2} & 2\tau_{\alpha x}\tau_{\alpha y} & \tau_{\alpha y}^{\,2} \\ n_x\tau_{\alpha x} & 2n_y\tau_{\alpha x} + n_x\tau_{\alpha y} & 2n_y\tau_{\alpha y} \\ 1 & 0 & 1 \end{pmatrix} \times \begin{pmatrix} \left[\partial^2 u/\partial x^2\right] \\ \left[\partial^2 u/\partial x\partial y\right] \\ \left[\partial^2 u/\partial y^2\right] \\ \left[\partial^2 v/\partial x^2\right] \\ \left[\partial^2 v/\partial x\partial y\right] \\ \left[\partial^2 v/\partial y^2\right] \end{pmatrix}$$

$$= -\begin{pmatrix} \partial\tau_{\alpha x}/\partial\alpha & \partial\tau_{\alpha y}/\partial\alpha & 0 & 0 \\ 2\partial n_x/\partial\alpha & \partial n_y/\partial\alpha & \partial n_y/\partial\alpha & 0 \\ 0 & 0 & 0 & 0 \\ 0 & 0 & \partial\tau_{\alpha x}/\partial\alpha & \partial\tau_{\alpha y}/\partial\alpha \\ 0 & \partial n_x/\partial\alpha & \partial n_x/\partial\alpha & 2\partial n_y/\partial\alpha \\ 0 & 0 & 0 & 0 \end{pmatrix} \begin{pmatrix} \left[\partial u/\partial x\right] \\ \left[\partial u/\partial y\right] \\ \left[\partial v/\partial x\right] \\ \left[\partial v/\partial y\right] \end{pmatrix}$$

$$+ \begin{pmatrix} \partial^2 q_x/\partial\alpha^2 \\ \partial R_{vx}/\partial\alpha \\ \mathrm{Re}\left\{\left[\partial p/\partial x\right] + \left[\rho\right]/\left[\mu\right]\partial q_x/\partial t\right\} \\ \partial^2 q_y/\partial\alpha^2 \\ \partial R_{vy}/\partial\alpha \\ \mathrm{Re}\left\{\left[\partial p/\partial y\right] + \left[\rho\right]/\left[\mu\right]\partial q_y/\partial t\right\} \end{pmatrix}, \tag{20}$$

$$\begin{pmatrix} \tau_{\alpha x}^{\,2} & 2\tau_{\alpha x}\tau_{\alpha y} & \tau_{\alpha y}^{\,2} \\ n_x\tau_{\alpha x} & n_x\tau_{\alpha y} + n_y\tau_{\alpha x} & n_y\tau_{\alpha y} \\ 1 & 0 & 1 \end{pmatrix} \begin{pmatrix} \left[\partial^2 p/\partial x^2\right] \\ \left[\partial^2 p/\partial x\partial y\right] \\ \left[\partial^2 p/\partial y^2\right] \end{pmatrix}$$

$$= \begin{pmatrix} \partial^2 R_p/\partial\alpha^2 \\ \partial R_{pn}/\partial\alpha \\ R_{pl} \end{pmatrix} - \begin{pmatrix} \partial\tau_{\alpha x}/\partial\alpha & \partial\tau_{\alpha y}/\partial\alpha \\ \partial n_x/\partial\alpha & \partial n_y/\partial\alpha \\ 0 & 0 \end{pmatrix} \begin{pmatrix} \left[\partial p/\partial x\right] \\ \left[\partial p/\partial y\right] \end{pmatrix}, \tag{21}$$

where the new quantities appearing on the right hand sides of the above equations are defined by:

$$R_{vx} = \mathrm{Re}\left(\frac{f_n n_x - f_x}{J}\right) - 2\left(\frac{\partial q_x}{\partial\tau}\tau_x + \frac{\partial q_y}{\partial\tau}\tau_y\right)n_x, \tag{22}$$

$$R_{vy} = \mathrm{Re}\left(\frac{f_n n_y - f_y}{J}\right) - 2\left(\frac{\partial q_x}{\partial\tau}\tau_x + \frac{\partial q_y}{\partial\tau}\tau_y\right)n_y, \tag{23}$$

$$R_p = \frac{f_n}{J} + \frac{2}{\mathrm{Re}}\left(\left[\frac{\partial u}{\partial x}\right]n_x^{\,2} + \left[\frac{\partial u}{\partial y}\right]n_y n_x + \left[\frac{\partial v}{\partial x}\right]n_x n_y + \left[\frac{\partial v}{\partial y}\right]n_y^{\,2}\right), \tag{24}$$

$$\begin{aligned} R_{pn} = {} & \frac{1}{J}\frac{\partial f_\alpha}{\partial\alpha} + \frac{2}{\mathrm{Re}}\frac{\partial}{\partial\tau}\left(\left[\frac{\partial u}{\partial x}\right]\right)n_x\tau_x \\ & + \frac{2}{\mathrm{Re}}\frac{\partial}{\partial\tau}\left(\left[\frac{\partial u}{\partial y}\right]\right)n_x\tau_y \\ & + \frac{2}{\mathrm{Re}}\frac{\partial}{\partial\tau}\left(\left[\frac{\partial v}{\partial x}\right]\right)n_y\tau_x + \frac{2}{\mathrm{Re}}\frac{\partial}{\partial\tau}\left(\left[\frac{\partial v}{\partial y}\right]\right)n_y\tau_y \\ & - \frac{\left[\rho\right]}{\left[\mu\right]}\left(\frac{\partial q_x}{\partial t}n_x + \frac{\partial q_y}{\partial t}n_y\right) + \frac{2}{\mathrm{Re}}\left[\frac{\partial u}{\partial x}\right]\frac{\partial}{\partial\tau}\left(n_x\tau_x\right) \\ & + \frac{1}{\mathrm{Re}}\left[\frac{\partial u}{\partial y}\right]\frac{\partial}{\partial\tau}\left(n_y\tau_x + n_x\tau_y\right) \\ & + \frac{1}{\mathrm{Re}}\left[\frac{\partial v}{\partial x}\right]\frac{\partial}{\partial\tau}\left(n_x\tau_y + n_y\tau_x\right) \\ & + \frac{2}{\mathrm{Re}}\left[\frac{\partial v}{\partial y}\right]\frac{\partial}{\partial\tau}\left(n_y\tau_y\right), \end{aligned} \tag{25}$$

$$R_{pl} = 2\left[\frac{\rho}{\mu^2}\left(\frac{\partial u}{\partial x}\frac{\partial v}{\partial y} - \frac{\partial u}{\partial y}\frac{\partial v}{\partial x}\right)\right], \tag{26}$$

$$f_n = f_x n_x + f_y n_y, \tag{27}$$

$$f_\alpha = \frac{f_x\tau_x + f_y\tau_y}{J}. \tag{28}$$

In addition to these equations, there is also the jump condition that follows from the continuity of the (non-scaled) velocity

$$\left[\mathbf{v}/\mu\right] = 0. \tag{29}$$

Now we describe a numerical technique to solve the above equations for all of the unknowns. Henceforth, for simplicity, we let $\rho^{+} = \rho^{-} = \rho$. Moreover, it is assumed that the force density $\mathbf{f}$ is either known a priori or determined by the local geometry of the singular curve. Fig. 2 shows a part of the Cartesian grid in the vicinity of the singular curve. Dashed lines represent grid lines, and

X's represent Lagrangian markers. Coordinate axes are taken as shown. Points K, M, N are grid points, while point L is the intersection of a grid line with the singular curve. Let $\left|\overline{KL}\right| = h^-$, $\left|\overline{LM}\right| = h^+$, and $\left|\overline{MN}\right| = h$.

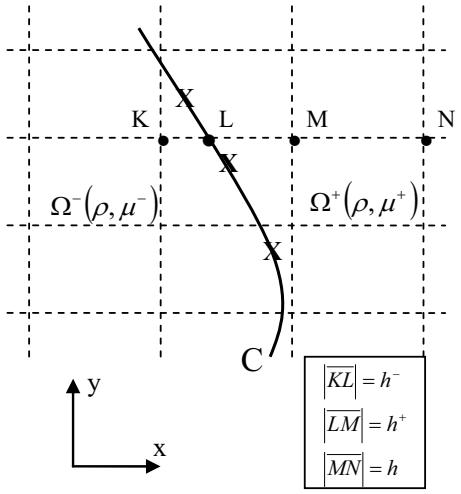

Fig.2 Part of the regular Cartesian grid in the neighborhood of the singular curve.

Applying Taylor expansion (truncated at third order) and eq. (29) at point L, the following three equations can be derived:

$$\left(\mu^+/[\mu]\right)\mathbf{q}_L + \left(h+h^+\right)\left(\partial\mathbf{v}/\partial x\right)_L^+ + \frac{\left(h+h^+\right)^2}{2}\left(\partial^2\mathbf{v}/\partial x^2\right)_L^+ = \mathbf{v}_N, \tag{30}$$

$$\left(\mu^+/[\mu]\right)\mathbf{q}_L + h^+\left(\partial\mathbf{v}/\partial x\right)_L^+ + \frac{h^{+2}}{2}\left(\partial^2\mathbf{v}/\partial x^2\right)_L^+ = \mathbf{v}_M, \tag{31}$$

$$\left(\mu^-/[\mu]\right)\mathbf{q}_L - h^-\left(\partial\mathbf{v}/\partial x\right)_L^+ + \frac{h^{-2}}{2}\left(\partial^2\mathbf{v}/\partial x^2\right)_L^+ = \mathbf{v}_K - h^-\left[\partial\mathbf{v}/\partial x\right]_L + \frac{h^{-2}}{2}\left[\partial^2\mathbf{v}/\partial x^2\right]_L. \tag{32}$$

If $\left[\partial\mathbf{v}/\partial x\right]_L$ and $\left[\partial^2\mathbf{v}/\partial x^2\right]_L$ are known, $\mathbf{q}_L$ can be obtained from these equations. Note that at every intersection point of a grid line with curve C, similar equations hold.

Notice that if $\mathbf{q}$ and $\mathbf{f}$ are known at all intersection points, provided that derivatives with respect to α can be obtained, eqs. (17)-(21) can be solved for the other jump conditions. However, despite the fact that $\mathbf{q}$ originally must be a smooth function of α, $\mathbf{q}$ obtained point-by-point from eqs. (30)-(32) contain numerical noise. To remove this noise, we use the cubic spline approximation with smoothing method developed by Woltring [9] to compute derivatives with respect to α.

Thus, eqs. (17)-(21) and (30)-(32) can be solved at all intersection points simultaneously by iterative computation. Assigning guess values for $\mathbf{q}$, eqs. (17)-(21) are solved for the remaining jump conditions. Subsituting these solutions in eqs. (30)-(32), new values for $\mathbf{q}$ are obtained. Using these as new guess values, the whole procedure is repeated again and again until convergence is achieved.

We emphasize here that obtaining $\mathbf{q}$ from eqs. (30)-(32) is an essential improvement to the interpolation technique in Ref.[8] to achieve sufficient accuracy. Since $\mathbf{q}$'s derivatives with respect to α have lower accuracy than $\mathbf{q}$ itself, it is important that $\mathbf{q}$ is interpolated with high (third order) accuracy. An example showing the improvement brought about by the new interpolation technique is given in the Appendix.

4. Numerical Test

To confirm the validity of the above technique, a numerical test is performed. We consider the steady circular flow shown in Fig. 3. Fluid Ω^+ and fluid Ω^- are separated by a circle C with radius a centered at the origin of coordinates O. C rotates steadily with angular velocity ω. A regular Cartesian grid $N_x \times N_y$, represented by dashed lines, encloses C. The grid's non-adjacent vertices are $A(-w,-w)$ and $B(w,w)$. (v_r, v_α) denotes the components of $\mathbf{v}$ in polar coordinates (r,α) and point P represents an arbitrary point within the grid.

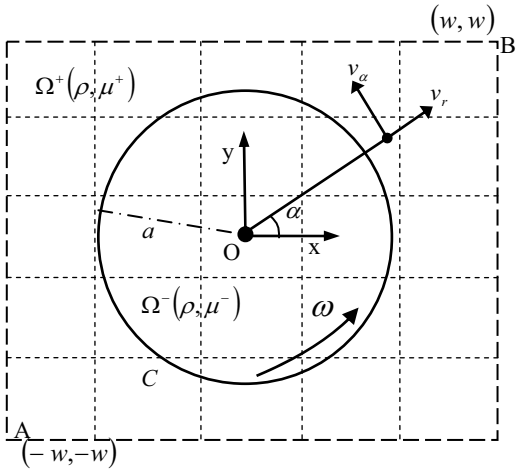

Fig.3 Steady flow of two fluids separated by a rotating circle. Dashed lines represent grid lines.

The analytical solution of the flow is given by

$v_r = 0, \quad v_\alpha = \mu^- \omega r,$

$$p = \frac{\rho\omega^2}{2} r^2, \qquad \text{for } r \le a. \quad (33)$$

$$v_r = 0, \quad v_\alpha = \frac{\mu^+ \omega a^2}{r},$$

$$p = -\frac{\rho\omega^2 a^4}{2r^2} + \rho\omega^2 a^2, \quad \text{for } r > a. \quad (34)$$

The force density acting on the circle is

$$f_n = 0 \quad , \quad f_\alpha = \frac{2}{\mathrm{Re}\, a^2} \mu^+ \omega, \quad (35)$$

At intersection points of grid lines with C, the force density is substituted. Then, we compute the jump conditions at the intersection points using the technique described in the previous section. These jump conditions are used to approximate spatial derivatives at neighboring points using the IIM discretization, i.e. eqs. (6) and (7). The IIM discretization is incorporated in a computational program for solving the governing equations. Our scheme uses the MAC method for time integration, and the SOR for solving the pressure Poisson equation. Using the analytical solution as initial and boundary conditions, we compute the time evolution of the circular flow until the singular curve makes one rotation.

Here, we show some results for parameters given as follows: $\mathrm{Re} = 3$, $a = 1$, $w = 1.5$, $\mu^- = 1$, $\mu^+ = 7$, $\omega = 1$, $\rho = 1$, $N_x = 50$, $N_y = 50$. Fig.4 shows the profiles of some of the jump conditions obtained. Horizontal axes represent α. Solid lines and dots represent analytical results and numerically obtained results, respectively. Figs. 4(a) and 4(b) show the profiles of q_x and q_y, respectively. Figs. 4(c) and 4(d) show the profiles of $\left[\partial u / \partial x\right]$ and $\left[\partial^2 u / \partial x^2\right]$, respectively. Figs. 4(e) and 4(f) show the profiles of $\left[\partial v / \partial y\right]$ and $\left[\partial^2 v / \partial y^2\right]$, respectively. It can be seen that the numerical results and the analytical results match very closely. This match is also obtained for the remaining jump conditions.

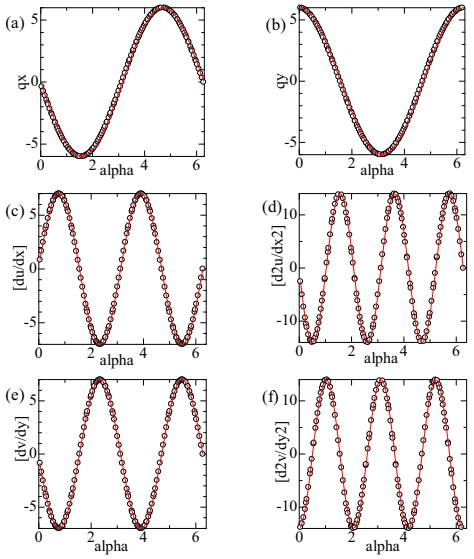

Fig.4 Profiles of jump conditions after one rotation of the singular curve. Horizontal axes represent α. Solid lines and dots represent analytical and numerically obtained results, respectively.

Fig.5 shows the profiles of some derivatives on a grid line $y = 0.3$ as an example. Horizontal axes represent x. Solid lines and dots represent analytical and numerical results, respectively. The intersection point is at $x \approx \pm 0.954$. Figs. 5(a) and 5(b) show the profiles of u and $\partial^2 u / \partial x^2$, respectively. Figs. 5(c) and 5(d) show the profiles of v and $\partial^2 v / \partial x^2$, respectively. Figs. 5(e) and 5(f) show the profiles of p and $\partial p / \partial x$, respectively. It can be seen that the numerical differentiations across the discontinuity approximate the analytical results well. On other grid lines, good approximations are also obtained.

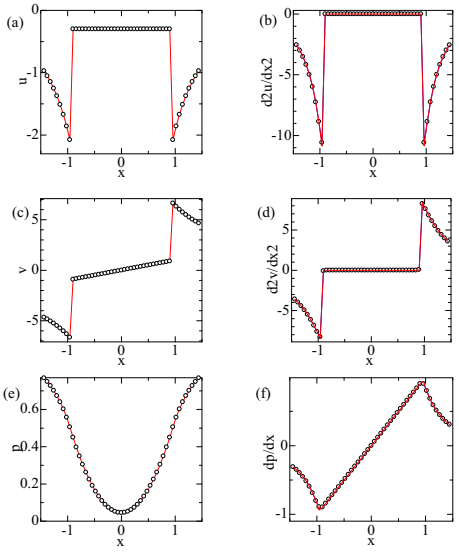

Fig.5 Profiles of some derivatives on a grid line after one rotation of the singular curve. Horizontal axes represent x. Solid lines and dots represent analytical and numerical results, respectively.

These results show that our formulations and the numerical technique work fairly well to approximate derivatives and solve the governing equations.

5. Concluding Remarks

The IIM technique proposed in Ref.[8] has been improved and tested numerically. The validity of the new formulation and the numerical technique has been confirmed by a numerical test of steady circular flow. Having established this, a numerical technique using the IIM discretization for non-steady flows is currently being developed. Due to limitation of space, we only show numerical test results for one set of parameters. However, it may be worth noting that the validity of our formulation and the numerical technique has also been confirmed for larger Reynolds numbers (small viscous term). The numerical oscillation of pressure jump condition is suppressed more easily, leading to better convergence. It suggests that our technique can be applied for high Reynolds number flows more easily than to low Reynolds number flows. We also consider that our method for neutral fluids can be extended to thermal plasmas. This extension is also under consideration.

Appendix

We provide Fig. 6 to show that the accuracy of the solutions of the equations of the jump conditions is improved by the new interpolation technique. We are concerned with the jump conditions at the initial time in the circular flow of section 4 here. Fig. 6 shows the profiles of the jump condition for the pressure and its derivatives. Blue lines represent numerical results obtained using the technique in ref. [8]. Red lines represent numerical results obtained using eqs. (30)-(32). Black lines (which coincide with the red lines) are analytical results. The order of magnitude represented by the red line is 10^{-5} in Fig. 6a, and 10^{-4} in Figs. 6b and 6c. It can be seen from Fig. 6 that numerical oscillations are suppressed more easily by using the new interpolation technique.

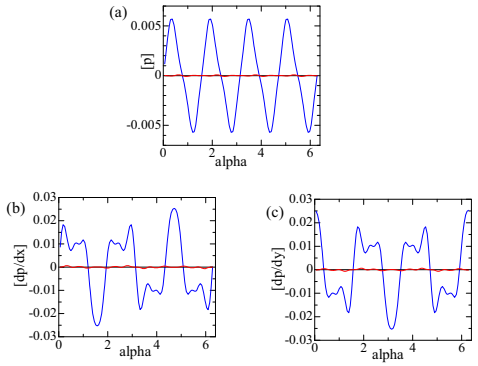

Fig.6 Profiles of jump conditions for the pressure and its derivatives at initial time. Same parameters as Figs. 4 and 5. Horizontal axes represent α. (a): the pressure, (b): the pressure's derivative with respect to x, (c): the pressure's derivative with respect to y. Blue lines represent numerical results obtained using the technique in ref. [8]. Red lines represent numerical results obtained using eqs. (30)-(32). Black lines (which coincide with the red lines) represent analytical results.

[1] H. Miura *et al.*, J. Plasma Physics 72, 1095 (2006).
[2] H. Miura *et al.*, Fusion Science and Technology 51, 8 (2007)
[3] M. Sato and N. Nakajima, Phys. Plasmas 13, 102507 (2006)
[4] K. Kusano *et al.*, Phys. Plasmas 5, 2582 (1998)
[5] Z. Li and K. Ito, The Immersed Interface Method, SIAM Frontiers in Applied Mathematics (2006) ch.1
[6] S. Xu and Z. Jane Wang, SIAM J. Sci. Comput. 27, 1948 (2006)
[7] S. Xu and Z. Jane Wang, J. Comput. Phys. 216, 454 (2006)
[8] Caesar O. Harahap and Hideaki Miura, Plasma Fusion Res. 3, S1052 (2008)
[9] Herman J. Woltring, Adv. Engng. Softw. 8, 104 (1986)